Carbon 238 (2025) 120156

Contents lists available at ScienceDirect

Carbon

journal homepage: www.elsevier.com/locate/carbon

Research paper

How does intercalation affect the structure and dynamics of bilayer graphene?

Noah J. Hourigan [a,*], Philipp Seiler [a], Maxwell Wetherington [b], Chengye Dong [c], Joshua A. Robinson [d], Giorgio Benedek [e,f], Anton Tamtögl [a,*]

[a] Institute of Experimental Physics, Graz University of Technology, 8010 Graz, Austria
[b] Materials Research Institute, The Pennsylvania State University, University Park, PA 16802, USA
[c] 2D Crystal Consortium, Materials Research Institute, The Pennsylvania State University, University Park, PA 16802, USA
[d] Materials Science and Engineering, Physics, Chemistry, 2D Crystal Consortium, Materials Research Institute, The Pennsylvania State University, University Park, PA 16802, USA
[e] Dipartimento di Scienza dei Materiali, Università di Milano-Bicocca, Via R. Cozzi 53, 20125 Milano, Italy
[f] Donostia International Physics Center (DIPC), Paseo de Lardizabal 4, 20018 Donostia-San Sebastian, Spain

ARTICLE INFO

Keywords:
Helium atom scattering
Electron-Phonon Coupling
Debye-Waller
Bilayer graphene
Thermal Expansion

ABSTRACT

The intercalation of graphene on silicon carbide (SiC) does not only offer the possibility to study unique two-dimensional polar metals such as Ga, it also provides a route to tune the properties of graphene-based systems and develop novel materials with tailored functionalities. Herein, we present a study of how the intercalation affects the surface structure and dynamics of bilayer graphene (BLG) on SiC, by comparing epitaxial BLG grown from a silicon carbide substrate, with a 2D gallium intercalated sample, and a hydrogen intercalated sample. Using Helium Atom Scattering (HAS), we probe surface characteristics such as the in-plane thermal expansion, the surface electronic corrugation, and the atom-surface interaction potential. Moreover, the electron–phonon (e-ph) coupling strength is determined from the thermal attenuation of specular helium scattering. Due to HAS probing exclusively the top-most graphene layer, we establish an unusually large negative thermal expansion, while the e-ph coupling is slightly larger than the values found for metal-supported single layer graphene. Despite the surface sensitivity of HAS we are also able to detect subtle differences likely to be related to the varying characteristics of the intercalated materials beneath.

1. Introduction

Since the isolation of graphene [1] there has been a growing interest into its modification and modulation in order to establish unique two-dimensional (2D) materials [2–9]. Recently, it was demonstrated that large-area, environmentally stable, single-crystal 2D metals such as gallium and others can be stabilised at the interface of epitaxial graphene and silicon carbide (SiC) via intercalation [10,11] (see Fig. 1(c)).

Atomically thin 2D metals are key ingredients in next-generation quantum and optoelectronic devices [10]. The mentioned intercalation approach allows to stabilise 2D metals against environmental degradation and thus further integration into heterostructure devices at the wafer scale [10,12]. Moreover, intercalation also enables both doping and decoupling of graphene from bulk substrates [13–15]. On the other hand, the photonic properties of 2D metals are also particularly interesting for second harmonic generation — as illustrated from air-stable 2D polar metals such as gallium and indium [16]. The study of non-linear optical properties and optoelectronic applications of these 2D heterostructures, as well as their characterisation though Raman spectroscopy [17], can greatly benefit from the simultaneous information on the structure, dynamics and electron–phonon interaction that can be extracted from a strictly surface-sensitive probe such as He atom scattering (HAS).

Here we report a HAS study of a bilayer graphene (BLG) on a 6H-SiC(0001) substrate, which is made quasi-freestanding via a carbon buffer layer (Fig. 1(a)), an intercalated atomic hydrogen passivating layer (Fig. 1(b)), or a 2D polar gallium bilayer (Ga_2, Fig. 1(c)). Note that the buffer layer cannot be considered as a third graphene layer due to the considerable sp^3 hybridised sites present, though this could be obtained through further evaporation of Si [18]. The gallium Ga_2 should be considered as a quasi-bilayer as the extent of the intercalation varies across the lateral interface but averages to approximately two layers (see 2.1 and Sample synthesis and characterisation in the

* Corresponding authors.
E-mail addresses: n.j.hourigan@tugraz.at (N.J. Hourigan), tamtoegl@tugraz.at (A. Tamtögl).

https://doi.org/10.1016/j.carbon.2025.120156
Received 11 November 2024; Received in revised form 17 February 2025; Accepted 21 February 2025
Available online 5 March 2025

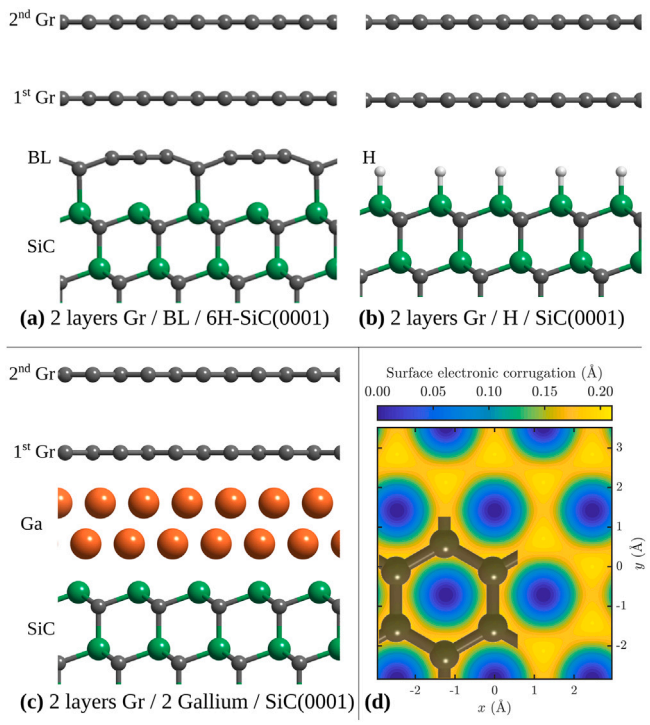

Fig. 1. Schematic illustration of the three sample structures. Parts (a)–(c) depict side views of the intercalated bilayer graphene systems. Finally, (d) shows a top down view of the surface electronic corrugation, overlayed with a partial atomic model of graphene.

supplementary information). This is a reasonable approximation given the large (3 mm diameter) spot size of the He beam cf. Ga grains on the scale of μm (see Figure S2 in the Supplementary Information).

By means of a HAS analysis, we compare the effects of the three different intercalations, focusing on surface structure, electronic corrugation, thermal expansion and the e-ph coupling i.e. the connection between the electronic and ionic system via thermal surface vibrations at finite temperature. HAS is particularly interesting as it is strictly surface sensitive [19–21] and exhibits a high sensitivity for the quality of single-crystalline surfaces and adsorbates [22–26].

Many previous experimental studies employ Raman spectroscopy, e.g., for studies of the lattice vibrational modes of graphene and its derivatives [27–30]. Of particular note to this work, is the use of Raman to detect signatures of AB-stacked bilayer graphene, which typically show a 2D band with a single pronounced minimum [31,32]. The I_{2D}/I_G ratio of ≈1 observed in Raman mapping is indicative of AB-stacked bilayer graphene [33]. Raman spectroscopy has also been used to study the effects of doping and intercalation on the electronic properties of bilayer graphene [34,35], and is further used for 2D-materials beyond graphene, such as transition metal dichalcogenides and topological insulators (TIs) [17,36,37] as well as intercalated 2D polar metals [38,39]. All of the above systems share the feature of being layered materials stacked by van der Waals interactions [36,40,41], and are therefore characterised by a prominent role of z-polarised acoustic phonons with a quasi-parabolic dispersion [42–44].

2. Methods

2.1. Sample preparation

All samples of this study were synthesised at the Materials Research Institute at Pennsylvania State University, following similar protocols as described in Ref. [10]. The intercalation of Ga is identified through low-frequency Raman features, which are unique spectral fingerprints for each metal intercalant, and then further correlated with optical contrast in micrographs to provide thickness information as further described in [38], as well as with further details and characterisation being given in Sample synthesis and characterisation of the supporting information. The stability of these intercalated films has also been subject to previous studies [10] and it is expected that the coverage does not show any significant changes over the time period of this study. All three samples were attached onto a sample plate using thermally and electrically conductive epoxy, which was cured by baking at 130 °C for a few minutes. The sample plates were then inserted into a transfer chamber using a load-lock system [45], from which they are further transferred into the sample holder of the scattering chamber. The sample holder itself can be cooled via a thermal connection to a liquid nitrogen reservoir and heated using a button heater. Before performing scattering measurements the samples were mildly annealed to promote desorption of any adsorbates but other than that no additional preparation protocols were performed which confirms the inert nature of the graphene layers.

2.2. Experimental details

HAS measurements were performed by scattering a nearly monochromatic beam of He ($\Delta E/E \approx 2\%$) off the sample surface in a fixed 91.5° source-sample-detector geometry (for a detailed description refer to Ref. [46]). Angular diffraction scans (ϑ-scans) were produced by rotating the sample in the scattering plane to yield different incident angles. Conversion to parallel momentum transfer ΔK follows from

$$\Delta K = |\Delta \mathbf{K}| = |\mathbf{K}_f - \mathbf{K}_i| = |\mathbf{k}_i| \left(\sin\vartheta_f - \sin\vartheta_i\right) \quad , \tag{1}$$

with $\mathbf{k}_i$ being the incident wave vector and ϑ_i and ϑ_f the incident and final angles with respect to the surface normal, respectively.

2.3. Close-coupling calculations

The electronic corrugation of the sample surfaces can be calculated using quantum mechanical scattering calculations, based on the close-coupling (CC) formalism. The CC formalism is a theoretical framework used to describe the elastic scattering of He atoms from surfaces. It is more exact than the hard-wall approximation whilst retaining a computationally manageable performance profile [47,48]. These calculations function through solving the CC equations [47] via the Numerov and Fox-Goodwin algorithms with the relevant boundary conditions [49].

The approach requires considering all open channels, where a standard scattering process occurs, as well as a limited number of closed channels, where the incident He atom transitions into a bound state. The end goal is to find the corrugation amplitude ξ_0 that minimises the deviation, R, between the simulated and experimental diffraction intensities, I_G^{SIM} and I_G^{exp}, with N the number of total experimentally measured diffraction scans:

$$R = \frac{1}{N}\sqrt{\sum_G \left(I_G^{\mathrm{exp}} - I_G^{\mathrm{sim}}\right)^2} \quad . \tag{2}$$

The simulated diffraction intensities are the result of the CC calculations which solve a set of coupled differential equations, stemming from the time-independent Schrödinger equation in combination with an atom-surface interaction potential, in the current case the corrugated Morse potential (CMP) [41]. For the CC calculations in this work we have take into account all open channels and 110 closed channels. The z-boundaries of the integration were set to $[-6, 18]$. Finally, the corrugation amplitude was varied between 0.05 and 0.45 Å.

3. Results and discussion

HAS measurements of highly-ordered pyrolytic graphite (HOPG) including the atom-surface interaction and surface phonons date back to the late 70s [50,51]. More recently, HAS has been employed for experimental studies of graphene and 2D-materials grown *in-situ* on metal substrates using chemical vapour deposition [52–56]. Those include the phonon dispersion of single layer graphene (SLG) [57,58], accounts of the coupling to the substrate from thermal attenuation measurements [59] as well as the bending rigidity of bilayer graphene (BLG) [60,61]. In addition to the mentioned Raman studies in the introduction, structural studies of graphene and BLG systems are mostly based on X-ray scattering using crystal truncation rods (CTRs) and low energy electron diffraction (LEED) studies, e.g., the stacking of single-layer graphene on Ni has been determined using CTRs [62]. However, due to the nature of X-ray scattering it will also probe beyond the initial surface layer and grazing incidence X-ray scattering is typically sensitive to the out-of-plane lattice constant c. [3,63]. On the other hand, LEED patterns have been used to identify the in-plane lattice constant and orientation of AB-stacked bilayer graphene without rotational misalignment, indicating single-crystalline growth [64,65], in contrast to twisted bilayer graphene with different twist angles [66]. Expanding on the content provided by these studies, based on HAS measurements we start with an analysis on the surface structure and electronic corrugation of the 3 BLG samples.

3.1. Surface structure and thermal expansion

Strictly speaking, the BLG on 6H-SiC(0001) cannot be classified as free-standing, as it is substrate-supported. However, the BLG samples grown on a SiC(0001) surface, after being passivated either by the formation of a carbon buffer layer (BL) or by hydrogen saturation (Fig. 1(a, b)) are currently termed in the literature as quasi-free standing (QFS) [13–15,67,68], due to reduced interlayer bonding to the substrate and modest deviations of the BLG work function ($\phi = 4.30$ eV and 4.71 eV, respectively [69]) with respect to that of graphite ($\phi =$ 4.55 eV [69]). The same BL effect is obtained by inserting two layers of Ga (Fig. 1(c)) whose work function in its metallic state is just 4.32 eV [67]. An electron or hole charge transfer from the substrate to the BLG occurs, according to whether ϕ is larger or smaller than that of graphite, by producing an increase or decrease of the surface charge density corrugation — an effect that HAS can reveal thanks to its very high sensitivity and resolution.

The structure of the BLG on a buffer layer graphene 6H-SiC(0001) [70,71] and hydrogen intercalated quasi-freestanding graphene have both been subject to previous studies [2]. In-plane structural information is mostly based on LEED, while the AB (bernal) stacking of the 2 graphene layers as well as the layer spacing follows from photoelectron diffraction [71]. LEED has also been used to identify the stacking order and, in some cases, suppression of a buffer layer and substrate upon intercalation of foreign elements [65,66,72].

The in-plane surface lattice constant a for all three samples of graphene on 6H-SiC(0001) was evaluated by averaging over several ϑ-scans along the $\overline{\Gamma M}$ direction (see Fig. 2), which have been converted to parallel momentum transfer (Eq. (1), in 2.2). The surface lattice constant, a, of BLG has been determined independently in the three samples at both room (296 K) and low (113 K) temperature following:

$$a = \frac{4\pi}{\sqrt{3}|G_{hk}|}\ ,\ |G_{hk}| = 2|k_i|\cos\left(\frac{\vartheta_{SD}}{2}\right)\sin\left(\frac{\vartheta_{SD}}{2} - \vartheta_i\right)\ . \tag{3}$$

These values were derived from the HAS diffraction spectra along the $\overline{\Gamma M}$ azimuth, and are collated in Table 1.

While the uncertainties of these values places them within each other, a clear trend is seen when considering all measurements made, as also exemplified in Fig. 2. The room temperature measurements in Table 1, show a good agreement with values for the bulk (graphite) lattice constant at room temperature reported in the literature (2.459 Å) [73]. At 113 K the lattice constants have expanded considerably, to higher values than previous literature of the bulk material would suggest [74], and in the context of quasi-free standing BLG it is more interesting to consider the thermal expansion.

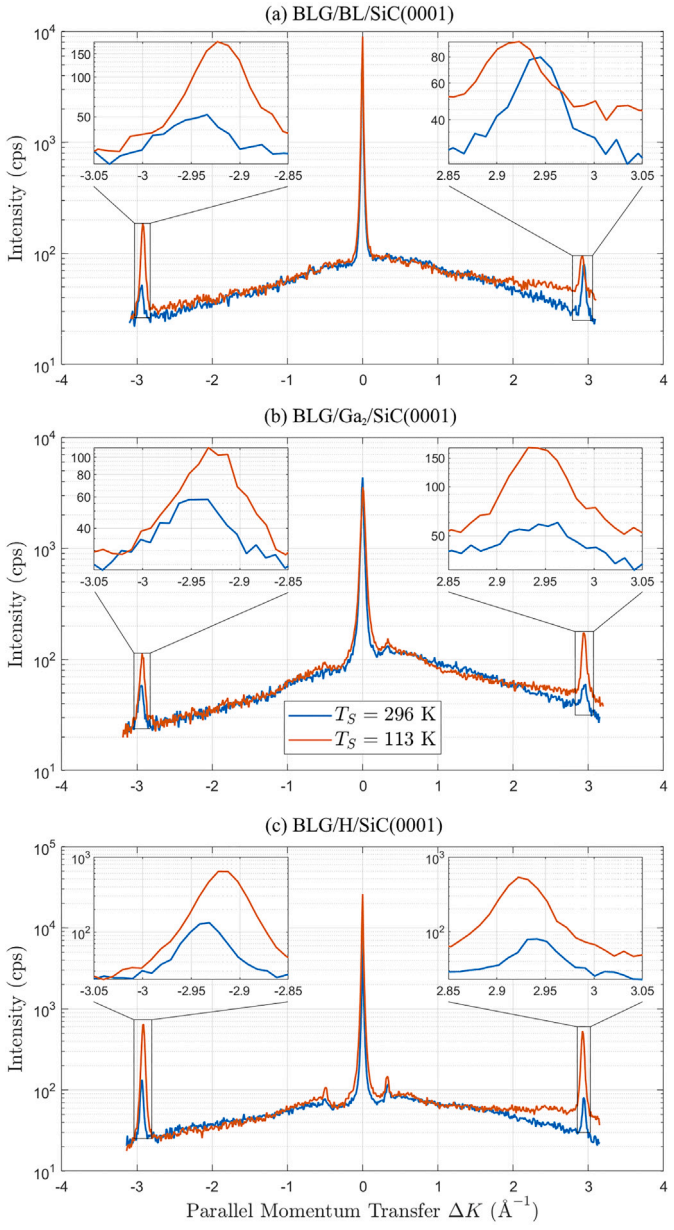

Fig. 2. Exemplary diffraction scans along $\overline{\Gamma M}$ of (a) BLG/BL/SiC, (b) BLG/Ga_2/SiC, and (c) BLG/H/SiC. The incident beam energy E_i is 13 meV. Measurements were made at room temperature, 296 K (blue) and low temperature, 113 K (red). The shift of the first order diffraction peaks is showcased within the insets, demonstrating the negative thermal expansion with increasing temperature. The satellite peaks seen in (c) are due to selective adsorption resonances. (For interpretation of the references to colour in this figure legend, the reader is referred to the web version of this article.)

It is well established that graphite exhibits a negative in-plane thermal expansion below 600 K [75,76], while this behaviour is less clear in suspended graphene. Experimentally, it has been shown that suspended graphene displays a negative in-plane thermal expansion below 350 K [77], however, this is in contrast with earlier density functional theory (DFT) calculations, which predicted a negative in-plane thermal expansion through 2300 K [78].

Table 1
Comparison of the in-plane lattice constant and the surface electronic corrugation for the three intercalated BLG systems. Both have been obtained at 113 K and at room temperature (296 K). The lattice constant has been determined from several diffraction scans according to (3), while the surface electronic corrugation is obtained via close-coupling calculations (see text). The last column lists the corresponding work functions of the SiC substrate with the BL, Ga_2 or H according to literature, illustrating the correlation with the trend of increasing surface electronic corrugation.

Sample	Lattice constant (Å)		Peak to peak corrugation (Å)		Work function (eV)
	113 K	296 K	113 K	296 K	
BLG/BL/SiC(0001)	2.48 ± 0.01	2.47 ± 0.01	0.21 ± 0.01	0.14 ± 0.01	4.30
BLG/Ga_2/SiC(0001)	2.47 ± 0.02	2.46 ± 0.01	0.22 ± 0.01	0.14 ± 0.01	4.32[a]
BLG/H/SiC(0001)	2.49 ± 0.01	2.47 ± 0.01	0.28 ± 0.01	0.23 ± 0.01	4.71

[a] Value given for metallic Ga [67].

The negative thermal expansion in graphene is attributed to its unique vibrational modes, particularly the out-of-plane thermal fluctuations, that dominate its thermal response [77,79]. Graphite also exhibits a negative yet smaller in-plane thermal expansion while the thermal expansion of the c-axis is positive, highlighting anisotropic thermal behaviour influenced by interlayer interactions [80]. These interactions complicate the thermal response, raising the question of how this behaviour affects the here studied BLG samples.

Assuming a linear thermal expansion behaviour, the thermal expansion coefficient $\alpha_\parallel$ (TEC) can be estimated according to $\alpha_\parallel = \frac{\Delta a}{a_0 \Delta T}$. Due to the relatively large uncertainties, we start by considering an average across all three investigated samples, calculated at:

$$\alpha_\parallel = (-2.33 \pm 0.88) \cdot 10^{-5}\,\mathrm{K}^{-1} \quad .$$

This is evidence of a thermal expansion coefficient an order of magnitude larger than for the bulk material, graphite, [76] or theoretical studies of suspended BLG [81]. On the other hand, it is in perfect agreement with studies of free-standing single-layer graphene, were the average TEC between 100 K and room temperature was estimated to be as large as $-2 \cdot 10^{-5}\,\mathrm{K}^{-1}$ [82]. Thus, it further illustrates that the thermal expansion and properties of the here studied intercalated BLG samples can indeed be considered as quasi-free standing (cf. the TEC of 6H-SiC which is $3.1 \cdot 10^{-6}\,\mathrm{K}^{-1}$ according to Stockmeier et al. [83]). Finally, our results do show some variation between each sample due to the effects of the intercalated materials. For example, BLG/Ga_2/SiC shows the smallest absolute value of (negative) thermal expansion due to the Ga quasi-bilayer expanding positively.

Due to the large difference between the Ga thermal expansion and the negative TEC of the BLG it is expected that the BLG will undergo significant lattice strain if the temperature is increased over a much larger scale. This can lead to the graphene layers buckling upon the cooling of the materials or slipping upon warming which can substantially increase the difficulty of gaining accurate measurements for the lattice constant and by extension the TEC [84]. Notably however, Yoon et al. demonstrated that BLG on a SiO_2 substrate does not slip until 400 K. They also found that buckling may occur at approximately 200 K [85]. On the one hand, it is difficult to determine if this is the case with our samples due to the limited number of temperatures the lattice constants were measured at. On the other hand it seems more likely that such buckling effects would be evident in vibrational spectra such as Raman spectra rather than directly influence the lattice spacing.

Finally, we also note that irrespective of strain introduced via thermal expansion, strain may also occur at the interface between the substrate and the graphene layer or the intercalated material, due to a lattice mismatch. For example, high-resolution LEED studies of single graphene layers on SiC indicate in-plane strain of 0.3–0.5% [86] and for the BLG/Ga_2/SiC sample it was shown that the Ga region is under moderate tensile strain (see Supplementary Information of [10]). It should be noted that the surface charge can reveal an interface lattice mismatch, if any, via diffraction from the associated Moiré pattern. This has recently been observed, e.g., for a $NbSe_2$ monolayer on BLG [87], but is apparently not the case here.

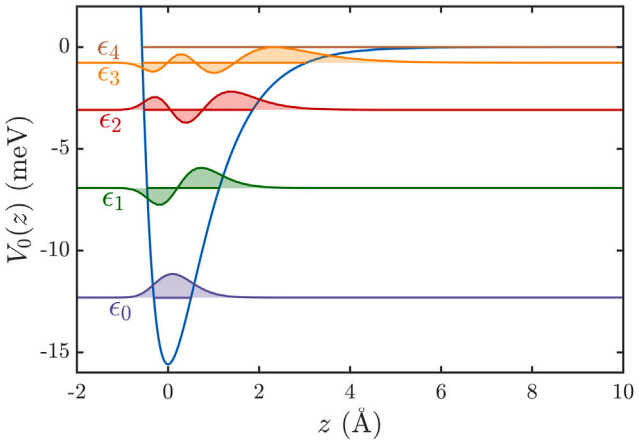

Fig. 3. The laterally averaged Morse potential of the He interaction with the BLG/H/SiC(0001) sample, obtained from SAR measurements. Bound states and their corresponding wavefunctions are also shown. The potential well depth is (15.59 ± 0.10) meV and the stiffness (1.21 ± 0.02) Å^{-1}. The wavefunction for ϵ_4 has been removed for clarity.

3.2. Surface electronic corrugation

Before determining the surface electronic corrugation, we shortly describe the atom-surface interaction potential, which is also a necessary prerequisite for the former as well as for any quantitative description and theoretical treatment of molecular adsorption or surface reactions [88]. Due to its interaction mechanism, HAS provides direct experimental information about the vdW interaction between an atom and the surface and thus invaluable details about London dispersion forces of vdW layered materials [41].

Atom-surface potential

As shown previously, for semimetal surfaces the He-surface interaction potential can be well described by a CMP [41,89,90]. Under the free-atom approximation, an incident He atom enters the attractive part of the potential and can become "trapped" upon which it will move freely parallel to the surface of the potential until such time that a further scattering event causes it to eject. This phenomenon is known as a selective adsorption resonance (SAR) and can be easily identified when looking at the intensity of the scattered He beam as a function of the incident beam energy [41].

The energies at which these fluctuations in He intensity occur correspond to the eigenenergies of the, now laterally averaged, Morse potential according to the free-atom approximation. Once the eigenenergies have been determined, they can be used to determine further characteristics of the laterally averaged Morse potential, i.e. χ, the stiffness parameter, and, D, the potential well depth. These potential parameters are a necessary ingredient for the CC calculations, in order to determine the surface electronic corrugation [41]. An exemplary laterally averaged Morse potential is shown in Fig. 3.

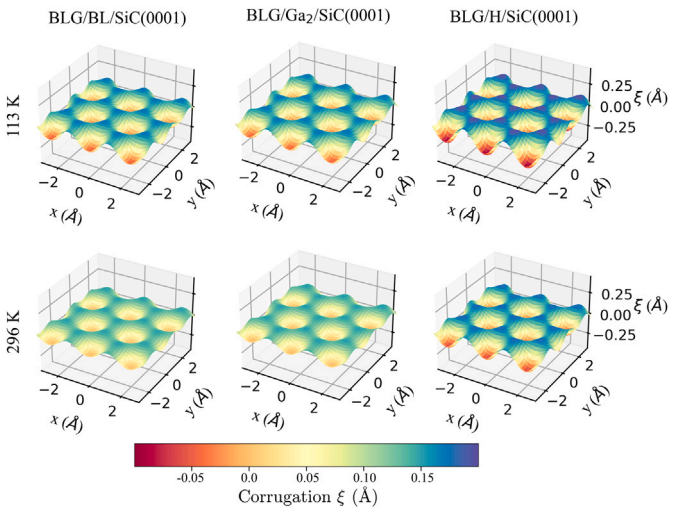

Fig. 4. Corrugation of the surface electron density, as "seen" by the He atoms. The corrugation follows the periodicity of the topmost graphene layer, as also shown in the contour plot of Fig. 1(d) with a partial atomic model of graphene. The average kinetic energy of the incident He beam was 11.3 meV and while the corrugation of all three samples is of the same order of magnitude, the H-passivated sample shows a significantly larger corrugation. A comparison between the lower row at room temperature and the top row (113 K) illustrates changes of the corrugation with temperature.

All three samples were found to have potential well depths within (15.5 ± 0.1) meV [91]. D is thus comparable to the parameters found for highly-ordered pyrolytic graphite (HOPG), with $D = 15.7$ meV [92]. Among the known atom-surface interaction potentials for semimetals [41], both graphene and graphite exhibit thus clearly the deepest potential well. As the well depth is mostly determined by the polarisability of the top-most layers, we do not see any significant difference between the three samples, and would further like to note, that a precise analysis of SAR features is beyond the scope of the current manuscript [91],

Surface electronic corrugation

The electronic corrugation of the sample surfaces was calculated using quantum mechanical scattering calculations, based on the CC algorithm (see 2.3). The scattering intensities obtained from the CC algorithm are then corrected for the effects of Debye–Waller attenuation upon comparison with experimental data taken at a finite temperature T_S. Finally, the calculated electronic corrugation is iteratively refined in order to minimise the deviation in intensities from experimental results (see 2.3). The surfaces and their corrugations are shown in Fig. 4, while the peak-to-peak corrugations are summarised in Table 1.

The amplitude of the electronic corrugation of graphene depends on the charge redistribution and the consequent graphene-substrate bonding strength. For example, graphene on Ni(111) has a particularly strong interaction [93], consistent with a large overlap with the free surface charge of Ni(111) and a very low corrugation of just 0.06 Å [55]. In contrast, for graphene on Rh(111) the interaction is six times smaller [93] and in combination with a small overlap, a corrugation as large as 0.90 Å is observed, which is related to the formation of a corrugated Moiré under these conditions [54]. In the present case, the SiC(0001) dangling-bond passivation by hydrogen reduces dramatically the graphene-substrate interaction so as to yield quasi-freestanding conditions. This is supported by our results where BLG/H/SiC, with a peak-to-peak corrugation of 0.23 Å, shows good agreement with literature, when compared to the surface electronic corrugation of HOPG at 0.21 Å, though measured with HAS at a lower surface temperature of 80 K [51].

Conversely, upon the intercalation of the gallium quasi-bilayer or the production of the carbon buffer layer, with work functions outside of a graphene environment of $\phi = 4.32$ eV and $\phi = 4.30$ eV respectively [69], a charge transfer to the BLG overlayer ($\phi = 4.71$ eV for quasi-freestanding BLG) is permitted. This has the effect of reducing the observed electronic corrugation to 0.14 Å, as indicated above. As displayed in the lower and upper row of Fig. 4, upon cooling the surface to 113 K, the samples show a significant increase of their corrugation: 57% for BLG/Ga_2/SiC, and 50% for BLG/BL/SiC, while the sample with BLG on H-passivated SiC(0001) shows a smaller increase of its corrugation equal to 22%.

When considering the peak-to-peak corrugation as a percentage of the graphene lattice constant ($a = 2.46$ Å), the values for the room temperature samples are 9.2% for BLG/H/SiC and 5.7% for BLG/BL/SiC and BLG/Ga_2/SiC. When the samples are cooled, the corrugations increase to 11.1% and 8.3% respectively. The increase of the corrugation with decreasing temperature is ascribed to the diminished effect of the thermal smoothing of the surface charge density. However, in the samples where there is some appreciable charge transfer, the reduction in peak-to-peak amplitude (8.3% → 5.7%, i.e., −31%) is approximately twice as fast as that of the H-passivated sample (11.1% → 9.2%, i.e., −17%). This is explained by additional contribution from the thermal excitations of electrons across the Fermi level.

Scanning Tunnelling Microscopy (STM) has also provided insights into the atomic-scale structure of BLG [86]. For BLG on Ru, it was shown that the top layer follows the Moiré pattern of the first graphene layer due to the lattice mismatch with the Ru substrate. This Moiré pattern leads to alternating AA and AB stacking across a 3 nm periodicity [94] and consequently also to a much larger corrugation. However, our systems have been shown to be exclusively AB stacking [7] and there is no evidence for any Moiré in the diffraction patterns. On the other hand, graphene on SiC exhibits minimal corrugation, with STM measurements showing a "roughness" of ≈0.16 Å for SLG and 0.09 Å for BLG, decreasing with layer number [95]. Since the corrugation strongly depends on the probing mechanism and e.g. in terms of STM on details such as the tip, a comparison to HAS should be treated with care. Nevertheless, we note that the "roughness" of the graphene/SiC system found in STM measurements is similar to our values of the surface electronic corrugation.

3.3. The Debye–Waller factor and electron–phonon coupling

In terms of He atom scattering, the Debye–Waller (DW) factor describes the attenuation of the elastically scattered intensity $I(T)$ due to the thermal atomic motion observed at temperature T, with respect to the elastic intensity of the corresponding rigid surface I_0 via $I(T) = I_0 \exp[-2W(T)]$. From the slope of the linear fit, at intermediate temperatures in Fig. 5, the Debye–Waller factor can be calculated, the results of which are listed in Table 2.

Considerable efforts have been made by the condensed matter community to study energy dissipation via e-ph coupling in materials. A convenient parameter to characterise the e-ph coupling strength is the mass-enhancement factor, λ [96]. Since the e-ph coupling describes the interaction between the electronic system and the lattice dynamics (phonons), experimental studies at finite temperature can either concentrate on the electronic or the phononic system. The former is mostly available via angle-resolved photoemission spectroscopy (ARPES) by examining the renormalisation of the electron energy dispersion in the vicinity of the Fermi surface due to e-ph interactions. The latter can be carried out using HAS, which on the contrary, studies the renormalisation of the surface phonon dispersion due to e-ph interactions. Furthermore, both techniques can be used to map out the phonon dispersion of a surface; however they do so on different energy scales [97].

As shown in recent works [98–101], the temperature dependence of the DW-exponent plotted in Fig. 5 permits to extract for a conducting

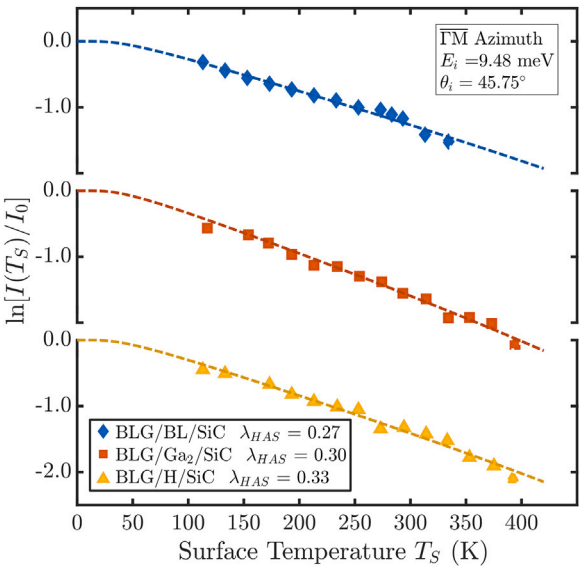

Fig. 5. The temperature dependence of the Debye–Waller exponent of the specular peak with all samples aligned along the $\overline{\Gamma M}$ azimuth. The dashed lines show the best-fit results according to Eq. (4), which allow the extraction of the electron–phonon coupling constant λ_{HAS}.

surface the mass-enhancement parameter λ. Since a He beam with energies in the meV region is scattered on a conducting surface by the surface free-electron density, the exchange of energy with the phonon gas occurs via the phonon-induced modulation of the surface electron gas, i.e., via the e–ph interaction. Therefore, the DW-factor, originating from the integrated action of all phonons weighted by their respective Bose factors, turns out to be directly proportional, under reasonable approximations and assumptions, to the mass-enhancement factor λ [93,100].

The DW-factor can be related to the mass-enhancement factor through the following equation [102]:

$$2W(T) = \frac{a_c k_{iz}^2}{\pi\phi} n_s \lambda_{HAS} \left\{ A\hbar\omega_1 \coth\left(\frac{\hbar\omega_1}{2k_B T}\right) + (1-A)\hbar\omega_2 \coth\left(\frac{\hbar\omega_2}{2k_B T}\right) \right\} . \quad (4)$$

Eq. (4) describes a combination of two phonon branches, one acoustic and one optical, of which the relative contribution of each can be adjusted through the parameter A [102]. Varying this parameter allows the best fit to the experimental data to be achieved, at which point λ can be evaluated. Hence, the mass-enhancement factor λ_{HAS} follows from (4), with $a_c = 5.20\,\text{Å}^2$ the unit cell area of the graphene overlayer, ϕ the work function and $k_{iz} = 2.97\,\text{Å}^{-1}$ the normal component of the incident wave vector. However, it is important to include the Beeby correction in these calculations. This correction adjusts the energy of the incoming He atoms to account for the attractive part of the potential felt by the He atom when approaching the surface [19] and thus increases the effective k_{iz} to $5.82\,\text{Å}^{-1}$. The work function, ϕ, is equal to 4.30 eV, 4.32 eV and 4.71 eV for BLG/BL/SiC, BLG/Ga$_2$/SiC, and BLG/H/SiC respectively [67,69]. n_s is the number of conducting layers which contribute to the phonon-induced modulation of the surface charge density and A is the above mentioned weighting factor which determines the relative contribution of the acoustic and optical phonon modes. Here, $\hbar\omega_1 = 10$ meV is the low energy acoustic phonon mode [103] and $\hbar\omega_2 = 160$ meV is the energy of the optical A_1' phonon mode [104].

As illustrated by the dashed lines in Fig. 5, the best fit to our experimental data is obtained at a value of $A = 0.65$, indicating a significant contribution from the low-energy acoustic phonon modes in our sample, whilst the optical A_1' appears to be much less active. This is supported by the negative thermal expansion discussed earlier in this paper, as it is widely established that the origin for that phenomenon in graphene relates to the large negative Grüneisen parameters found in graphenes lowest energy, highly-populated, transverse acoustic ZA mode [78,105].

Table 2
Comparison of the Debye–Waller factor and electron–phonon coupling characteristics for the three studied BLG systems with different intercalations. Additional single layer graphene (SLG) system studies have been included for further context.

Sample	Debye–Waller factor ($\cdot 10^{-3}$ K^{-1})	λ_{HAS}	Refs.
BLG/BL/SiC(0001)	5.0 ± 0.7	0.27 ± 0.01	
BLG/Ga$_2$/SiC(0001)	6.6 ± 0.3	0.30 ± 0.01	
BLG/H/SiC(0001)	6.7 ± 0.5	0.33 ± 0.01	
SLG/Ni(111)	–	0.06	[93]
SLG/Ru(111)	–	0.05	[93]

The extracted λ_{HAS} values for all three BLG samples are summarised in Table 2. While, to the best of our knowledge, there are currently no values reported for the experimental determination of λ in BLG systems, Park et al. have produced a study focused on this through first-principles calculations [103]. They found that BLG, at the maximum doping considered, will show an approximate 30% increase in λ compared to SLG, ($\lambda = 0.28$ c.f. $\lambda = 0.21$) which is in excellent agreement with the values we have found here.

Conversely, Calandra et al. who first noted the presence of the 160 meV A_1' mode as well as a 195 meV E_{2g} mode, found a value of $\lambda = 0.02$ [104]. This is also closer to the value found by Pound et al. in a study on theoretical free-standing SLG with a value of $\lambda = 0.07$, though this is in relation to an optical phonon mode of even greater energy [106]. One of the few experimental studies in this area was performed by Zhou et al. [107]. Their experiment focused on an ARPES study of the epitaxial graphene A_1' mode, the same as Calandra's theory study, but found an almost order of magnitude larger value at $\lambda = 0.14$ [107]. The most likely explanation for this divergence between theoretical and experimental results is due to the electron–electron interaction not considered in the calculations [104].

Finally, from temperature-dependent Raman measurements of intercalated 2D gallium an abrupt increase of the linewidth at ≈280 K was reported, likely to be associated with an abrupt change of the e-ph coupling strength [108]. Since the HAS measurements do not show any significant changes at the mentioned temperature, it appears likely that HAS is not sensitive enough to these phononic contributions form the intercalated Ga layer. In other words, since HAS is probing the surface charge density above the topmost layer, any contribution of these modes [39] to the e-ph coupling in the intercalated Ga layer does not seem to be significant enough to be reflected in our measurements of λ_{HAS}. Compared to ARPES studies of single layer graphene, where it was shown that the e-ph can be increased by as much as a factor of 10 upon intercalation [109], we further anticipate based on our results that the effect of intercalation on the e-ph coupling in BLG is much less pronounced. Due to the apparent surface sensitivity of HAS it may further provide benchmark data for recently developed fully ab initio approaches of inelastic scattering [110], where e.g. it has been shown that the atomic-scale surface structure affects and reduces e-ph coupling and superconductivity on Nb compared to its bulk [111].

4. Summary and conclusion

We have reported a comparative helium atom scattering study of a bilayer graphene (BLG) on a 6H-SiC(0001) substrate, for (i) a carbon buffer layer (BL) between BLG and SiC, (ii) an intercalated 2D polar gallium quasi-bilayer and (iii) an intercalated atomic hydrogen layer. Here, we focus on surface characteristics of the BLG, specifically the thermal expansion, the electronic corrugation, and the

electron–phonon coupling. The intercalated materials exhibit distinct influences on the surfaces properties of BLG. The findings show that intercalation alters both the in-plane thermal expansion and electronic corrugation, with the hydrogen-passivated sample demonstrating the largest effects. Furthermore, we report the strong influence of low-energy acoustic phonon modes on e-ph interactions, providing evidence of enhanced electron–phonon coupling in BLG systems (λ_{HAS} in the range 0.27–0.33) in comparison with previous studies of single layer graphene samples (λ_{HAS} in the range 0.05–0.06) [93]. These results contribute to a deeper understanding of intercalation effects, paving the way for further exploration of 2D-materials in advanced quantum and optoelectronic applications.

We hope that the herein presented experimental approach and data will stimulate further research, e.g. by including different intercalated metals. Further studies would also benefit from investigating how these properties are effected by the extent of intercalated species coverage. For example, whether reducing the 2D Ga bilayer to a monolayer will significantly influence the binding strength of the BLG. However, due to the inherent stability of these materials there is no simple process to precisely control this coverage.

CRediT authorship contribution statement

Noah J. Hourigan: Writing – review & editing, Writing – original draft, Visualization, Validation, Investigation, Formal analysis, Data curation. **Philipp Seiler:** Writing – review & editing, Investigation, Data curation, Validation. **Maxwell Wetherington:** Writing – review & editing, Resources, Validation. **Chengye Dong:** Writing – review & editing, Resources. **Joshua A. Robinson:** Writing – review & editing, Funding acquisition. **Giorgio Benedek:** Writing – review & editing, Supervision, Formal analysis. **Anton Tamtögl:** Writing – review & editing, Visualization, Supervision, Project administration, Methodology, Investigation, Funding acquisition, Formal analysis, Conceptualization.

Acknowledgements

This research was funded in whole, or in part, by the Austrian Science Fund (FWF) [10.55776/P34704]. This work is supported by the Penn State MRSEC Center for Nanoscale Science via the National Science Foundation (NSF) award DMR-2011839 and the Penn State 2DCC-MIP under NSF cooperative agreement DMR-2039351. For the purpose of open access, the author has applied a CC BY public copyright licence to any Author Accepted Manuscript version arising from this submission.

Declaration of competing interest

The authors declare that they have no known competing financial interests or personal relationships that could have appeared to influence the work reported in this paper.

Appendix A. Supplementary data

Additional details on sample synthesis including characterisation figures are in the supplementary information.

Supplementary material related to this article can be found online at https://doi.org/10.1016/j.carbon.2025.120156.

References

[1] K.S. Novoselov, A.K. Geim, S.V. Morozov, D. Jiang, Y. Zhang, S.V. Dubonos, et al., Electric field effect in atomically thin carbon films, Science 306 (5696) (2004) 666–669, http://dx.doi.org/10.1126/SCIENCE.1102896.

[2] C. Riedl, C. Coletti, T. Iwasaki, A.A. Zakharov, U. Starke, Quasi-free-standing epitaxial graphene on SiC obtained by hydrogen intercalation, Phys. Rev. Lett. 103 (2009) 246804, http://dx.doi.org/10.1103/PhysRevLett.103.246804.

[3] C. Riedl, C. Coletti, U. Starke, Structural and electronic properties of epitaxial graphene on SiC(0001): a review of growth, characterization, transfer doping and hydrogen intercalation, J. Phys. D: Appl. Phys. 43 (37) (2010) 374009.

[4] K. Kanetani, K. Sugawara, T. Sato, R. Shimizu, K. Iwaya, T. Hitosugi, et al., Ca intercalated bilayer graphene as a thinnest limit of superconducting C_6Ca, Proc. Natl. Acad. Sci. USA 109 (48) (2012) 19610–19613, http://dx.doi.org/10.1073/PNAS.1208889109.

[5] B.J. Schultz, R.V. Dennis, V. Lee, S. Banerjee, An electronic structure perspective of graphene interfaces, Nanoscale 6 (7) (2014) 3444–3466, http://dx.doi.org/10.1039/C3NR06923K.

[6] Y. Cao, V. Fatemi, S. Fang, K. Watanabe, T. Taniguchi, E. Kaxiras, P. Jarillo-Herrero, Unconventional superconductivity in magic-angle graphene superlattices, Nature 556 (2018) 43–50, http://dx.doi.org/10.1038/nature26160.

[7] N. Briggs, Z.M. Gebeyehu, A. Vera, T. Zhao, K. Wang, A.D.L.F. Duran, B. Bersch, T. Bowen, K.L. Knappenberger, J.A. Robinson, Epitaxial graphene/silicon carbide intercalation: a minireview on graphene modulation and unique 2d materials, Nanoscale 11 (2019) 15440–15447, http://dx.doi.org/10.1039/C9NR03721G.

[8] Y. Lei, T. Zhang, Y.-C. Lin, T. Granzier-Nakajima, G. Bepete, D.A. Kowalczyk, et al., Graphene and beyond: Recent advances in two-dimensional materials synthesis, properties, and devices, ACS Nanosci. Au 2 (6) (2022) 450–485, http://dx.doi.org/10.1021/acsnanoscienceau.2c00017.

[9] C. Li, Y.-F. Zhao, A. Vera, O. Lesser, H. Yi, S. Kumari, et al., Proximity-induced superconductivity in epitaxial topological insulator/graphene/gallium heterostructures, Nat. Mater. (2023) http://dx.doi.org/10.1038/s41563-023-01478-4.

[10] N. Briggs, B. Bersch, Y. Wang, J. Jiang, R.J. Koch, N. Nayir, K. Wang, M. Kolmer, W. Ko, A.D.L.F. Duran, S. Subramanian, C. Dong, J. Shallenberger, M. Fu, Q. Zou, Y.W. Chuang, Z. Gai, A.P. Li, A. Bostwick, C. Jozwiak, C.Z. Chang, E. Rotenberg, J. Zhu, A.C. van Duin, V. Crespi, J.A. Robinson, Atomically thin half-van der waals metals enabled by confinement heteroepitaxy, Nat. Mater. 19 (6) (2020) 637–643, http://dx.doi.org/10.1038/s41563-020-0631-x, 19 (2020).

[11] H. El-Sherif, N. Briggs, B. Bersch, M. Pan, M. Hamidinejad, S. Rajabpour, et al., Scalable characterization of 2D gallium-intercalated epitaxial graphene, ACS Appl. Mater. Interfaces 13 (46) (2021) 55428–55439, http://dx.doi.org/10.1021/acsami.1c14091.

[12] S. Wundrack, D. Momeni, W. Dempwolf, N. Schmidt, K. Pierz, L. Michaliszyn, et al., Liquid metal intercalation of epitaxial graphene: Large-area gallenene layer fabrication through gallium self-propagation at ambient conditions, Phys. Rev. Mater. 5 (2) (2021) 024006, http://dx.doi.org/10.1103/PHYSREVMATERIALS.5.024006.

[13] H. Kim, O. Dugerjav, A. Lkhagvasuren, J.M. Seo, Charge neutrality of quasi-free-standing monolayer graphene induced by the intercalated Sn layer, J. Phys. D 49 (13) (2016) 135307, http://dx.doi.org/10.1088/0022-3727/49/13/135307.

[14] J.C. Kotsakidis, A. Grubišić-Čabo, Y. Yin, A. Tadich, R.L. Myers-Ward, M.T. Dejarld, et al., Freestanding n-doped graphene via intercalation of calcium and magnesium into the buffer layer–SiC(0001) interface, Chem. Mater. 32 (15) (2020) 6464–6482, http://dx.doi.org/10.1021/ACS.CHEMMATER.0C01729.

[15] M. Kolmer, W. Ko, J. Hall, S. Chen, J. Zhang, H. Zhao, et al., Breaking of inversion symmetry and interlayer electronic coupling in bilayer graphene heterostructure by structural implementation of high electric displacement fields, J. Phys. Chem. Lett. 13 (2022) 11571–11580, http://dx.doi.org/10.1021/ACS.JPCLETT.2C02407.

[16] M.A. Steves, Y. Wang, N. Briggs, T. Zhao, H. El-Sherif, B.M. Bersch, S. Subramanian, C. Dong, T. Bowen, A.D.L.F. Duran, K. Nisi, M. Lassaunière, U. Wurstbauer, N.D. Bassim, J. Fonseca, J.T. Robinson, V.H. Crespi, J. Robinson, K.L. Knappenberger, Unexpected near-infrared to visible nonlinear optical properties from 2-D polar metals, Nano Lett. 20 (2020) 8312–8318, http://dx.doi.org/10.1021/ACS.NANOLETT.0C03481.

[17] X. Cong, X.-L. Liu, M.-L. Lin, P.-H. Tan, Application of Raman spectroscopy to probe fundamental properties of two-dimensional materials, npj 2D Mater. Appl. 4 (1) (2020) 13, http://dx.doi.org/10.1038/S41699-020-0140-4.

[18] T. Cavallucci, V. Tozzini, Intrinsic structural and electronic properties of the buffer layer on silicon carbide unraveled by density functional theory, Sci. Rep. 8 (1) (2018) 1–10, http://dx.doi.org/10.1038/s41598-018-31490-7, 8 (2018).

[19] D. Farías, K.-H. Rieder, Atomic beam diffraction from solid surfaces, Rep. Progr. Phys. 61 (12) (1998) 1575.

[20] G. Benedek, J.P. Toennies, Atomic Scale Dynamics at Surfaces, Springer Berlin Heidelberg, Berlin, Heidelberg, 2018, http://dx.doi.org/10.1007/978-3-662-56443-1.

[21] B. Holst, G. Alexandrowicz, N. Avidor, G. Benedek, G. Bracco, W.E. Ernst, et al., Material properties particularly suited to be measured with helium scattering: selected examples from 2D materials, van der Waals heterostructures, glassy materials, catalytic substrates, topological insulators and superconducting radio frequency materials, Phys. Chem. Chem. Phys. 23 (2021) 7653–7672, http://dx.doi.org/10.1039/D0CP05833E.

[22] G. Anemone, E. Climent-Pascual, H.K. Yu, A. Al Taleb, F. Jiménez-Villacorta, et al., Quality of graphene on sapphire: long-range order from helium diffraction versus lattice defects from Raman spectroscopy, RSC Adv. 25 (2016) 21235, http://dx.doi.org/10.1039/C5RA27452D.

[23] C. Lin, N. Avidor, G. Corem, O. Godsi, G. Alexandrowicz, G.R. Darling, et al., Two-dimensional wetting of a stepped copper surface, Phys. Rev. Lett. 120 (2018) 076101, http://dx.doi.org/10.1103/PhysRevLett.120.076101.

[24] A. Tamtögl, E. Bahn, M. Sacchi, J. Zhu, D.J. Ward, A.P. Jardine, et al., Motion of water monomers reveals a kinetic barrier to ice nucleation on graphene, Nat. Commun. 12 (2021) 3120, http://dx.doi.org/10.1038/s41467-021-23226-5.

[25] Nick A. von Jeinsen, Sam M. Lambrick, Matthew Bergin, Aleksandar Radić, Boyao Liu, Dan Seremet, Andrew P. Jardine, David J. Ward, 2D helium atom diffraction from a microscopic spot, Phys. Rev. Lett. 131 (2023) 236202, http://dx.doi.org/10.1103/PhysRevLett.131.236202.

[26] M. Sacchi, A. Tamtögl, Water adsorption and dynamics on graphene and other 2D materials: Computational and experimental advances, Adv. Phys.: X 8 (2023) 2134051, http://dx.doi.org/10.1080/23746149.2022.2134051.

[27] A.C. Ferrari, D.M. Basko, Raman spectroscopy as a versatile tool for studying the properties of graphene, Nat. Nanotechnol. 8 (4) (2013) 235–246, http://dx.doi.org/10.1038/NNANO.2013.46.

[28] P.H. Tan, W.P. Han, W.J. Zhao, Z.H. Wu, K. Chang, H. Wang, Y.F. Wang, N. Bonini, N. Marzari, N. Pugno, G. Savini, A. Lombardo, A.C. Ferrari, The shear mode of multilayer graphene, Nat. Mater. 11 (4) (2012) 294–300, http://dx.doi.org/10.1038/nmat3245.

[29] J.-B. Wu, X. Zhang, M. Ijäs, W.-P. Han, X.-F. Qiao, X.-L. Li, et al., Resonant Raman spectroscopy of twisted multilayer graphene, Nat. Commun. 5 (1) (2014) 5309, http://dx.doi.org/10.1038/NCOMMS6309.

[30] C. Cong, T. Yu, Enhanced ultra-low-frequency interlayer shear modes in folded graphene layers, Nat. Commun. 5 (1) (2014) 4709, http://dx.doi.org/10.1038/NCOMMS5709.

[31] S. Nie, W. Wu, S. Xing, Q. Yu, J. Bao, S.-s. Pei, K.F. McCarty, Growth from below: bilayer graphene on copper by chemical vapor deposition, New J. Phys. 14 (9) (2012) 093028, http://dx.doi.org/10.1088/1367-2630/14/9/093028.

[32] W. Fang, A.L. Hsu, R. Caudillo, Y. Song, A.G. Birdwell, E. Zakar, M. Kalbac, M. Dubey, T. Palacios, M.S. Dresselhaus, P.T. Araujo, J. Kong, Rapid identification of stacking orientation in isotopically labeled chemical-vapor grown bilayer graphene by Raman spectroscopy, Nano Lett. 13 (4) (2013) 1541–1548, http://dx.doi.org/10.1021/nl304706j.

[33] M. Fabiane, M.J. Madito, A. Bello, N. Manyala, Raman spectroscopy and imaging of bernal-stacked bilayer graphene synthesized on copper foil by chemical vapour deposition: growth dependence on temperature, J. Raman Spectrosc. 48 (5) (2017) 639–646, http://dx.doi.org/10.1002/jrs.5094.

[34] M. Kalbac, H. Farhat, J. Kong, P. Janda, L. Kavan, M.S. Dresselhaus, Raman spectroscopy and in situ Raman spectroelectrochemistry of bilayer $^{12}C/^{13}C$ graphene, Nano Lett. 11 (5) (2011) 1957–1963, http://dx.doi.org/10.1021/nl2001956.

[35] P. Gava, M. Lazzeri, A.M. Saitta, F. Mauri, Probing the electrostatic environment of bilayer graphene using Raman spectra, Phys. Rev. B 80 (15) (2009) 155422, http://dx.doi.org/10.1103/physrevb.80.155422.

[36] X. Lu, X. Luo, J. Zhang, S.Y. Quek, Q. Xiong, Lattice vibrations and Raman scattering in two-dimensional layered materials beyond graphene, Nano Res. 9 (2016) 3559–3597, http://dx.doi.org/10.1007/S12274-016-1224-5.

[37] L. Liang, J. Zhang, B.G. Sumpter, Q.-H. Tan, P.-H. Tan, V. Meunier, Low-frequency shear and layer-breathing modes in Raman scattering of two-dimensional materials, ACS Nano 11 (12) (2017) 11777–11802, http://dx.doi.org/10.1021/ACSNANO.7B06551.

[38] M.T. Wetherington, F. Turker, T. Bowen, A. Vera, S. Rajabpour, N. Briggs, S. Subramanian, A. Maloney, J.A. Robinson, 2-dimensional polar metals: a low-frequency Raman scattering study, 2D Mater. 8 (2021) 041003, http://dx.doi.org/10.1088/2053-1583/AC2245.

[39] W. He, M.T. Wetherington, K.A. Ulman, J.L. Gray, J.A. Robinson, S.Y. Quek, Shear modes in a 2D polar metal, J. Phys. Chem. Lett. 2022 (2022) 4015–4020, http://dx.doi.org/10.1021/ACS.JPCLETT.2C00719, graphene interacts with metals via Van der Waals.

[40] Y. Ando, Topological insulator materials, J. Phys. Soc. Japan 82 (10) (2013) 102001, http://dx.doi.org/10.7566/JPSJ.82.102001.

[41] A. Tamtögl, A. Ruckhofer, D. Campi, M. Bremholm, W.E. Ernst, P. Hofmann, et al., Atom-surface van der Waals potentials of topological insulators and semimetals from scattering measurements, Phys. Chem. Chem. Phys. 23 (2021) 7637–7652, http://dx.doi.org/10.1039/D0CP05388K.

[42] A. Tamtögl, D. Campi, M. Bremholm, E.M.J. Hedegaard, B.B. Iversen, M. Bianchi, et al., Nanoscale surface dynamics of Bi_2Te_3(111): Observation of a prominent surface acoustic wave and the role of van der Waals interactions, Nanoscale 10 (2018) 14627–14636, http://dx.doi.org/10.1039/C8NR03102A.

[43] A. Ruckhofer, D. Campi, M. Bremholm, P. Hofmann, G. Bendek, M. Bernasconi, W.E. Ernst, A. Tamtögl, THz surface modes and electron-phonon coupling in Bi_2Se_3(111), Phys. Rev. Res. 2 (2020) 023186, http://dx.doi.org/10.1103/PhysRevResearch.2.023186.

[44] P. Maier, N.J. Hourigan, A. Ruckhofer, M. Bremholm, A. Tamtögl, Surface properties of 1T-TaS_2 and and contrasting its electron-phonon coupling with $TlBiTe_2$ from helium atom scattering, Front. in Chem. 11 (2023) 1249290, http://dx.doi.org/10.3389/fchem.2023.1249290.

[45] A. Tamtögl, E.A. Carter, D.J. Ward, N. Avidor, P.R. Kole, A.P. Jardine, et al., Note: A simple sample transfer alignment for ultra-high vacuum systems, Rev. Sci. Instrum. 87 (2016) 066108, http://dx.doi.org/10.1063/1.4954728.

[46] A. Tamtögl, M. Mayrhofer-Reinhartshuber, N. Balak, W.E. Ernst, K.H. Rieder, Elastic and inelastic scattering of he atoms from Bi(111), J. Phys.: Condens. Matter. 22 (30) (2010) 304019.

[47] A.S. Sanz, S. Miret-Artés, Selective adsorption resonances: Quantum and stochastic approaches, 2007, http://dx.doi.org/10.1016/j.physrep.2007.08.001.

[48] W. Allison, S. Miret-Artés, E. Pollak, Perturbation theory of scattering for grazing-incidence fast-atom diffraction, Phys. Chem. Chem. Phys. 24 (2022) 15851–15859, http://dx.doi.org/10.1039/D2CP01013E.

[49] P. Kraus, A. Tamtögl, M. Mayrhofer-Reinhartshuber, G. Benedek, W.E. Ernst, Resonance-enhanced inelastic He-atom scattering from subsurface optical phonons of Bi(111), Phys. Rev. B 87 (2013) 245433, http://dx.doi.org/10.1103/PhysRevB.87.245433.

[50] H. Hoinkes, The physical interaction potential of gas atoms with single-crystal surfaces, determined from gas-surface diffraction experiments, Rev. Modern Phys. 52 (4) (1980) 933, http://dx.doi.org/10.1103/RevModPhys.52.933.

[51] G. Boato, P. Cantini, R. Tatarek, Study of gas-graphite potential by means of helium atom diffraction, Phys. Rev. Lett. 40 (1978) 887, http://dx.doi.org/10.1103/PhysRevLett.40.887.

[52] A. Ruckhofer, M. Sacchi, A.J.R. Payne, A.P. Jardine, W.E. Ernst, N.a.a. Avidor, Evolution of ordered nanoporous phases during h-BN growth: Controlling the route from gas-phase precursor to 2D material by in-situ monitoring, Nanoscale Horiz. 7 (2022) 1388–1396, http://dx.doi.org/10.1039/D2NH00353H.

[53] A.J.R. Payne, N.J.F. Xavier, A. Tamtögl, M. Sacchi, Unravelling the epitaxial growth mechanism of hexagonal and nanoporous boron nitride: A first-principles microkinetic model, Small – (2025) 2405404, http://dx.doi.org/10.1002/smll.202405404.

[54] K.D. Gibson, S.J. Sibener, Helium atom scattering from graphene grown on Rh(111), J. Phys. Chem. C 118 (2014) 29077–29083, http://dx.doi.org/10.1021/JP504024T.

[55] A. Tamtögl, E. Bahn, J. Zhu, P. Fouquet, J. Ellis, W. Allison, Graphene on Ni(111): Electronic corrugation and dynamics from helium atom scattering, J. Phys. Chem. C 119 (46) (2015) 25983–25990, http://dx.doi.org/10.1021/acs.jpcc.5b08284.

[56] H. Shichibe, Y. Satake, K. Watanabe, A. Kinjyo, A. Kunihara, Y. Yamada, M. Sasaki, W.W. Hayes, J.R. Manson, Probing interlayer interactions between graphene and metal substrates by supersonic rare-gas atom scattering, Phys. Rev. B 91 (2015) 155403, http://dx.doi.org/10.1103/PHYSREVB.91.155403.

[57] A. al Taleb, G. Anemone, D. Farías, R. Miranda, Acoustic surface phonons of graphene on Ni(111), Carbon 99 (2016) 416–422, http://dx.doi.org/10.1016/j.carbon.2015.12.043.

[58] A. Al Taleb, D. Farías, Phonon dynamics of graphene on metals, J. Phys.: Condens. Matter. 28 (10) (2016) 103005, http://dx.doi.org/10.1088/0953-8984/28/10/103005.

[59] A.A. Taleb, G. Anemone, R. Miranda, D. Farías, Characterization of interlayer forces in 2D heterostructures using neutral atom scattering, 2D Mater. 5 (4) (2018) 045002, http://dx.doi.org/10.1088/2053-1583/aacf26.

[60] S.D. Eder, S.K. Hellner, S. Forti, J.M. Nordbotten, J.R. Manson, C. Coletti, et al., Temperature-dependent bending rigidity of AB-stacked bilayer graphene, Phys. Rev. Lett. 127 (2021) 266102, http://dx.doi.org/10.1103/PhysRevLett.127.266102.

[61] M. Tømterud, S.K. Hellner, S.D. Eder, S. Forti, J.R. Manson, C. Colletti, et al., Temperature dependent bending rigidity of graphene, 2022, arXiv preprint arXiv:2210.17250.

[62] R. Rameshan, V. Vonk, D. Franz, J. Drnec, S. Penner, A. Garhofer, F. Mittendorfer, A. Stierle, B. Klötzer, Role of precursor carbides for graphene growth on Ni(111), Sci. Rep. 8 (1) (2018) 2662, http://dx.doi.org/10.1038/s41598-018-20777-4.

[63] P. Zielinski, M. Kühne, D. Kärcher, F. Paolucci, P. Wochner, S. Fecher, J. Drnec, R. Felici, J.H. Smet, Probing exfoliated graphene layers and their lithiation with microfocused X-rays, Nano Lett. 19 (6) (2019) 3634–3640, http://dx.doi.org/10.1021/acs.nanolett.9b00654.

[64] C. Yang, T. Wu, H. Wang, G. Zhang, J. Sun, G. Lu, T. Niu, A. Li, X. Xie, M. Jiang, Copper-vapor-assisted rapid synthesis of large AB-stacked bilayer graphene domains on Cu-Ni alloy, Small 12 (15) (2016) 2009–2013, http://dx.doi.org/10.1002/smll.201503658.

[65] T. Ohta, T.E. Beechem, J.T. Robinson, G.L. Kellogg, Long-range atomic ordering and variable interlayer interactions in two overlapping graphene lattices with stacking misorientations, Phys. Rev. B 85 (7) (2012) 075415, http://dx.doi.org/10.1103/physrevb.85.075415.

[66] S. Nie, A.L. Walter, N.C. Bartelt, E. Starodub, A. Bostwick, E. Rotenberg, K.F. McCarty, Growth from below: Graphene bilayers on Ir(111), ACS Nano 5 (3) (2011) 2298–2306, http://dx.doi.org/10.1021/nn103582g.

[67] W.M. Haynes, D.R. Lide, T.J. Bruno (Eds.), CRC Handbook of Chemistry and Physics, 95th Edition, CRC Press, 2014.

[68] K.M. Daniels, M.M. Jadidi, A.B. Sushkov, A. Nath, A.K. Boyd, K. Sridhara, H.D. Drew, T.E. Murphy, R.L. Myers-Ward, D.K. Gaskill, Narrow plasmon resonances enabled by quasi-freestanding bilayer epitaxial graphene, 2D Mater. 4 (2) (2017) 025034, http://dx.doi.org/10.1088/2053-1583/aa5c75.

[69] S. Mammadov, J. Ristein, J. Krone, C. Raidel, M. Wanke, V. Wiesmann, F. Speck, T. Seyller, Work function of graphene multilayers on SiC(0001), 2D Mater. 4 (2017) 015043, http://dx.doi.org/10.1088/2053-1583/4/1/015043.

[70] F. Fromm, M. Oliveira Jr., A. Molina-Sánchez, M. Hundhausen, J. Lopes, H. Riechert, L. Wirtz, et al., Contribution of the buffer layer to the Raman spectrum of epitaxial graphene on SiC(0001), New J. Phys. 15 (4) (2013) 043031.

[71] I. Razado-Colambo, J. Avila, D. Vignaud, S. Godey, X. Wallart, D. Woodruff, M. Asensio, Structural determination of bilayer graphene on SiC(0001) using synchrotron radiation photoelectron diffraction, Sci. Rep. 8 (1) (2018) 1–10, http://dx.doi.org/10.1038/s41598-018-28402-0.

[72] J. Kleeman, K. Sugawara, T. Sato, T. Takahashi, Enhancement of electron–phonon coupling in Cs-overlayered intercalated bilayer graphene, J. Phys.: Condens. Matter. 28 (20) (2016) 204001, http://dx.doi.org/10.1088/0953-8984/28/20/204001.

[73] Y. Baskin, L. Meyer, Lattice constants of graphite at low temperatures, Phys. Rev. 100 (1955) 544, http://dx.doi.org/10.1103/PhysRev.100.544.

[74] E.A. Kellett, B.P. Richards, The thermal expansion of graphite within the layer planes, J. Nucl. Mater. 12 (1964) 184–192, http://dx.doi.org/10.1016/0022-3115(64)90139-4.

[75] A.C. Bailey, B. Yates, Anisotropic thermal expansion of pyrolytic graphite at low temperatures, J. Appl. Phys. 41 (1970) 5088–5091, http://dx.doi.org/10.1063/1.1658609.

[76] J.E. Zorzi, C.A. Perottoni, Thermal expansion of graphite revisited, Comput. Mater. Sci. 199 (2021) 110719, http://dx.doi.org/10.1016/J.COMMATSCI.2021.110719.

[77] W. Bao, F. Miao, Z. Chen, H. Zhang, W. Jang, C. Dames, C.N. Lau, Controlled ripple texturing of suspended graphene and ultrathin graphite membranes, Nat. Nanotechnol. 4 (9) (2009) 562–566, http://dx.doi.org/10.1038/nnano.2009.191.

[78] N. Mounet, N. Marzari, First-principles determination of the structural, vibrational and thermodynamic properties of diamond, graphite, and derivatives, Phys. Rev. B 71 (2005) 205214, http://dx.doi.org/10.1103/PhysRevB.71.205214.

[79] D.T. Ho, H.S. Park, S.Y. Kim, U. Schwingenschlögl, Graphene origami with highly tunable coefficient of thermal expansion, ACS Nano 14 (7) (2020) 8969–8974, http://dx.doi.org/10.1021/acsnano.0c03791.

[80] V. Oddone, R.C. Wimpory, S. Reich, Understanding the negative thermal expansion in planar graphite–metal composites, J. Mater. Sci. 54 (2) (2018) 1267–1274, http://dx.doi.org/10.1007/s10853-018-2879-y.

[81] K.V. Zakharchenko, J.H. Los, M.I. Katsnelson, A. Fasolino, Atomistic simulations of structural and thermodynamic properties of bilayer graphene, Phys. Rev. B 81 (2010) 235439, http://dx.doi.org/10.1103/PHYSREVB.81.235439.

[82] W. Bao, K. Myhro, Z. Zhao, Z. Chen, W. Jang, L. Jing, F. Miao, H. Zhang, C. Dames, C.N. Lau, In situ observation of electrostatic and thermal manipulation of suspended graphene membranes, Nano Lett. 12 (11) (2012) 5470–5474, http://dx.doi.org/10.1021/nl301836q.

[83] M. Stockmeier, R. Müller, S.A. Sakwe, P.J. Wellmann, A. Magerl, On the lattice parameters of silicon carbide, J. Appl. Phys. 105 (2009) 033511, http://dx.doi.org/10.1063/1.3074301.

[84] P.R. Shaina, L. George, V. Yadav, M. Jaiswal, Estimating the thermal expansion coefficient of graphene: the role of graphene–substrate interactions, J. Phys.: Condens. Matter. 28 (2016) 085301, http://dx.doi.org/10.1088/0953-8984/28/8/085301.

[85] D. Yoon, Y.W. Son, H. Cheong, Negative thermal expansion coefficient of graphene measured by Raman spectroscopy, Nano Lett. 11 (2011) 3227–3231, http://dx.doi.org/10.1021/NL201488G.

[86] C. Berger, Z. Song, T. Li, X. Li, A.Y. Ogbazghi, R. Feng, Z. Dai, A.N. Marchenkov, E.H. Conrad, P.N. First, W.A. de Heer, Ultrathin epitaxial graphite: 2D electron gas properties and a route toward graphene-based nanoelectronics, J. Phys. Chem. B 108 (52) (2004) 19912–19916, http://dx.doi.org/10.1021/jp040650f.

[87] A.A. Taleb, W. Wan, G. Benedek, M.M. Ugeda, D. Farías, Electron–phonon coupling and phonon dynamics in single-layer $NbSe_2$ on graphene: the role of moiré phonons, ACS Nano (2025) http://dx.doi.org/10.1021/acsnano.4c16399.

[88] J. Bühler, J. Rocin, C. Brand, Describing the scattering of keV protons through graphene, Front. in Chem. 11 (2023) 1291065, http://dx.doi.org/10.3389/fchem.2023.1291065.

[89] M. Mayrhofer-Reinhartshuber, P. Kraus, A. Tamtögl, S. Miret-Artés, W.E. Ernst, Helium-surface interaction potential of Sb(111) from scattering experiments and close-coupling calculations, Phys. Rev. B 88 (2013) 205425, http://dx.doi.org/10.1103/PhysRevB.88.205425.

[90] P. Kraus, A. Tamtögl, M. Mayrhofer-Reinhartshuber, F. Apolloner, C. Gösweiner, S. Miret-Artés, W.E. Ernst, Surface structure of Bi(111) from helium atom scattering measurements, inelastic close-coupling formalism, J. Phys. Chem. C 119 (2015) 17235–17242, http://dx.doi.org/10.1021/ACS.JPCC.5B05010.

[91] N.J. Hourigan, P. Seiler, D. Campi, A. Tamtögl, Surface phonon dispersion and atom-surface interaction potential of intercalated bilayer graphene, 2025, in preparation.

[92] G. Boato, P. Cantini, C. Salvo, R. Tatarek, S. Terreni, Atomic vibrations at the (0001) graphite surface studied by he atom scattering, Surf. Sci. 114 (2) (1982) 485–497, http://dx.doi.org/10.1016/0039-6028(82)90700-2.

[93] G. Benedek, J.R. Manson, S. Miret-Artés, The electron–phonon coupling constant for single-layer graphene on metal substrates determined from he atom scattering, Phys. Chem. Chem. Phys. 23 (2021) 7575–7585, http://dx.doi.org/10.1039/D0CP04729E.

[94] J. Wagner, R. Edel, T. Grabnic, B. Wiggins, S.J. Sibener, On-surface chemical dynamics of monolayer, bilayer, many-layered graphene surfaces probed supersonic beam scattering STM imaging, Faraday Discuss. 251 (2024) 435–447, http://dx.doi.org/10.1039/d3fd00178d.

[95] Y. Murata, V. Petrova, I. Petrov, S. Kodambaka, In situ high-temperature scanning tunneling microscopy study of bilayer graphene growth on 6H-SiC(0001), Thin Solid Films 520 (16) (2012) 5289–5293, http://dx.doi.org/10.1016/j.tsf.2012.03.040.

[96] G. Grimvall, The Electron-Phonon Interaction in Metals, North-Holland Pub. Co, 1981.

[97] H.I. Røst, S.P. Cooil, A.C. Åsland, J. Hu, A. Ali, T. Taniguchi, K. Watanabe, B.D. Belle, B. Holst, J.T. Sadowski, F. Mazzola, J.W. Wells, Phonon-mediated quasiparticle lifetime renormalizations in few-layer hexagonal boron nitride, Nano Lett. 23 (16) (2023) 7539–7545, http://dx.doi.org/10.1021/acs.nanolett.3c02086.

[98] A. Tamtögl, P. Kraus, N. Avidor, M. Bremholm, E.M.J. Hedegaard, B.B. Iversen, et al., Electron–phonon coupling and surface debye temperature of Bi_2Te_3(111) from helium atom scattering, Phys. Rev. B 95 (2017) 195401, http://dx.doi.org/10.1103/PhysRevB.95.195401.

[99] S. G. Benedek, J.P. Toennies, Electron–phonon coupling constant of metallic overlayers from specular He atom scattering, J. Phys. Chem. Lett. 9 (1) (2018) 76–83, http://dx.doi.org/10.1021/acs.jpclett.7b03047.

[100] G. Benedek, S. Miret-Artés, J.R. Manson, A. Ruckhofer, W.E. Ernst, A. Tamtögl, Origin of the electron-phonon interaction of topological semimetal surfaces measured with helium atom scattering, J. Phys. Chem. Lett. 11 (5) (2020) 1927–1933.

[101] J.R. Manson, G. Benedek, S. Miret-Artés, Atom scattering as a probe of the surface electron–phonon interaction at conducting surfaces, Surf. Sci. Rep. 77 (2022) 100552, http://dx.doi.org/10.1016/j.surfrep.2022.100552.

[102] G. Benedek, J.R. Manson, S. Miret-Artés, The role of high-energy phonons in electron–phonon interaction at conducting surfaces with helium-atom scattering, Phys. Chem. Chem. Phys. 24 (2022) 23135–23141, http://dx.doi.org/10.1039/D2CP03501D.

[103] C.H. Park, F. Giustino, M.L. Cohen, S.G. Louie, Electron–phonon interactions in graphene, bilayer graphene, and graphite, Nano Lett. 8 (2008) 4229–4233, http://dx.doi.org/10.1021/NL801884N.

[104] M. Calandra, F. Mauri, Electron–phonon coupling and electron self-energy in electron-doped graphene: Calculation of angular-resolved photoemission spectra, Phys. Rev. B 76 (2007) 205411, http://dx.doi.org/10.1103/PHYSREVB.76.205411.

[105] S. Mann, R. Kumar, V.K. Jindal, Negative thermal expansion of pure and doped graphene, RSC Adv. 7 (36) (2017) 22378–22387, http://dx.doi.org/10.1039/C7RA01591G.

[106] A. Pound, J.P. Carbotte, E.J. Nicol, Phonon structures in the electronic density of states of graphene in magnetic field, Europhys. Lett. 94 (2011) 57006, http://dx.doi.org/10.1209/0295-5075/94/57006.

[107] S.Y. Zhou, D.A. Siegel, A.V. Fedorov, A. Lanzara, Kohn anomaly and interplay of electron–electron and electron–phonon interactions in epitaxial graphene, Phys. Rev. B 78 (2008) 193404, http://dx.doi.org/10.1103/PHYSREVB.78.193404.

[108] M.T. Wetherington, Inelastic Light Scattering and Lattice Dynamics of 2-Dimensional Polar Metals (Ph.d. thesis), Pennyslvania State University, 2021.

[109] C. Hwang, D.Y. Kim, D.A. Siegel, K.T. Chan, J. Noffsinger, A.V. Fedorov, M.L. Cohen, B. Johansson, J.B. Neaton, A. Lanzara, Ytterbium-driven strong enhancement of electron–phonon coupling in graphene, Phys. Rev. B 90 (2014) 115417, http://dx.doi.org/10.1103/PhysRevB.90.115417.

[110] M.M. Kelley, R. Sundararaman, T.A. Arias, Fully ab initio approach to inelastic atom-surface scattering, Phys. Rev. Lett. 132 (2024) 016203, http://dx.doi.org/10.1103/PhysRevLett.132.016203.

[111] C.J. Thompson, M.F. Van Duinen, M.M. Kelley, T.A. Arias, S.J. Sibener, Correlating electron-phonon coupling and in situ high-temperature atomic-scale surface structure at the metallic Nb(100) surface by Helium atom scattering and density functional theory, J. Phys. Chem. C 128 (14) (2024) 6149–6157, http://dx.doi.org/10.1021/acs.jpcc.4c00852.